



**„Babeş – Bolyai“ University of Cluj – Napoca
Faculty of Chemistry and Chemical Engineering**

**Kinetic and electrochemical methods of analysis by
means of enzyme and heterogeneous catalyzed
reactions**

Abstract of PhD Thesis

Florina Făgădar (Pogăcean)

**Scientific advisor:
Prof. Univ. Dr. Ioan Bâldea**

CLUJ-NAPOCA

2011

Abstract

This Ph.D. thesis approaches several kinetic studies and mechanism of enzymatic reaction, in the presence or absence of inhibitors and aims possible kinetic analysis of these inhibitors. In addition it presents original methods for preparation of chemically modified electrodes (with gold nanoparticles respectively graphene) for detection of various drugs. Chapter II and III presents the reaction of hydrogen peroxide decomposition in the presence of catalase and peroxidase, using either β -blocker drugs or phenol. as inhibitors Kinetic parameters are determined by means of both spectrophotometric and amperometric data. Chapter IV and V presents the morphological and electrochemical characteristics of modified electrodes and their possible application as sensor for atenolol and carbamazepine respectively.

**„Babeş – Bolyai“ University of Cluj – Napoca Faculty of
Chemistry and Chemical Engineering**

Florina Făgădar (Pogăcean)

**Kinetic and electrochemical methods of analysis by
means of enzyme and heterogeneous catalyzed
reactions**

Abstract of PhD Thesis

Jury:

Jury President:

Conf. Univ. Dr. Cornelia Majdik - dean

Scientific advisor:

Prof. Univ. Dr. Ioan Bâldea

Reviewers:

Prof. Univ. Dr. Elena Maria Pică- Technical University , Cluj-Napoca,

Conf. Dr. Graziella Liana Turdean- „Babeş – Bolyai“ University of Cluj –
Napoca Faculty of Chemistry and Chemical Engineering

C. P. I, Dr. Valer Almăşan – National Institute for Research and
Development of Isotopic and Molecular Technologies Cluj-Napoca, (INCDTIM).

Content

| | |
|--|-----------|
| INTRODUCTION | 1 |
| Chapter1. General consideration on enzyme catalyzed reactions and how to follow them | 4 |
| 1.1. Kinetics of enzymatic reactions..... | 4 |
| 1.2. Models of linearization | 7 |
| 1.3. Inhibition of enzymatic reactions..... | 10 |
| 1.4. Fraction of inhibition..... | 18 |
| 1.5. Models of reversible inhibition..... | 24 |
| 1.6. Graphical determination of inhibition type..... | 26 |
| 1.7. Some considerations about Clark oxygen sensors..... | 32 |
| 1.8. Some considerations about spectrophotometric methods..... | 34 |
| 1.9. General aspects of voltametry..... | 36 |
| 1.10. General aspects of impedance spectroscopy..... | 40 |
| Chapter 2.The inhibitory effect of phenol on the peroxidase–catalyzed decomposition of hydrogen peroxide | 44 |
| 2.1. Peroxidase: general presentation..... | 44 |
| 2.2. Classification of peroxidase..... | 46 |
| 2.3. Structure of enzyme..... | 48 |
| 2.4. Mechanism of peroxidase reaction..... | 50 |
| 2.5. Method of extraction and purification of horseradish peroxidase..... | 52 |
| 2.6. Kinetics reactions..... | 53 |
| Original contributions | |
| 2.7. Reagents and solutions..... | 54 |
| 2.8. Principle of aliens methode to horseradish peroxidase..... | 55 |
| 2.9. Principle of amperometric method..... | 55 |
| Conclusions | 64 |
| Chapter 3 Kinetic determination of drug concentration via enzyme-catalyzed decomposition of hydrogen peroxide | 65 |
| 3.1. Catalase : General presentation | 65 |
| 3.2. Mechanism of catalatic reaction..... | 66 |
| 3.3. Drug used as inhibitors of hydrogen peroxide decompositions of reactions ... | 67 |
| 3.4. β -blocker- drug. General .features..... | 70 |
| 3.5. Atenolol, Metoprolol.General presentation..... | 74 |
| 3.6. Farmacokinetics..... | 74 |
| 3.7. Effect of atenolol and metoprolol..... | 74 |
| Original contributions | |
| 3.8. Reagents and solutions..... | 75 |
| A) Spectrophotometric method for the determination of atenolol..... | 76 |
| 3.9. Results and discussions..... | 76 |
| B). Amperometric method for the determination of atenolol..... | 76 |
| 3.10. Results and discussions..... | 80 |
| A) Spectrophotometric method for the determination of metoprolol | 83 |
| 3.11. Results and discussions..... | 83 |
| B). Amperometric method for the determination of metoprolol..... | 85 |
| 3.12. Results and discussions..... | 85 |
| 3.13. The influence of environmetal factors on enzyme activity..... | 89 |
| Conclusions | 92 |
| Chapter 4 Study of Atenolol oxidation by using a glasy carbon electrode, modifield with multicomponent nanostructural assembly of amino acids and | 94 |

| | |
|--|------------|
| gold nanoparticles | |
| Original contributions | |
| Experimental part..... | 96 |
| 4.1 Reagents and solutions..... | 96 |
| 4.2. Preparation of citrate-capped gold nanoparticles (AuNPs)..... | 97 |
| 4.3. Preparation of GCE modified with AuNPs (GCE-AuNPs | 97 |
| 4.4. Equipment used..... | 98 |
| 4.5. Results and discussios..... | 99 |
| 4.6. Electrochemical characterization, GCE-AuNPs | 106 |
| Conclusions..... | 123 |
| Chapter 5. Novel Graphene-Gold Nanoparticle Modified Electrodes for the High Sensitivity Electrochemical Spectroscopy Detection and Analysis of Carbamazepine | |
| 5.1. General characteristics of carbamazepine | 124 |
| 5.2. Reagents and solutions..... | 128 |
| 5.3. Preparation of gold electrode modified with graphene-AuNPs (Au-GR-AuNPs) | 128 |
| 5.4. Equipment used..... | 129 |
| 5.5. Results and discussios..... | 130 |
| 5.6. Electrochemical caracterization, Au-Gr-AuNPs | 132 |
| Conclusions..... | 144 |
| Generale conclusions | 145 |
| References..... | 147 |

Keywords: catalase, peroxidase, drug inhibitors, modified electrodes, gold nanoparticles

Introduction

The purpose of this paper is to study the kinetic and electrochemical method of analysis of some drugs, based on enzyme and heterogeneous catalyzed reaction

This thesis consists of five chapters:

The first chapter presents theoretical aspects related to enzyme catalyzed reaction and the way they are being followed. Here are presented the General aspects of enzymatic reaction kinetics, the used linearization models inhibition of enzymatic reaction and type of inhibitors, inhibition fraction. It is also referred to analytic methods used spectrophotometric, amperometric, voltammetric method, impedance spectroscopy.

The second chapter is devoted to study the process of inhibition by phenol of the decomposition of H_2O_2 reaction, catalyzed by peroxidase. Both measurements were made with pure peroxidase and horseradish peroxidase extracted.

We determine kinetic parameters, inhibition constants for phenol, and establish the inhibition mechanism. A method of horseradish peroxidase extraction was developed.

The third chapter presents the decomposition of hydrogen peroxide in the presence of catalase using two drugs as inhibitors (atenolol, metoprolol)

Here we have determined the kinetic parameters, inhibition constants for both atenolol and metoprolol, by spectrophotometric method and amperometric method. Inhibition mechanism was also established for the two β -blocking medicines, atenolol and metoprolol.

We tried to develop some kinetic methods methods of these drugs determination.

Chapter 4 presents the study of atenolol oxidation using a glassy carbon electrode, GCE, whose surface was modified with amino acids and gold nanoparticles, by linear voltammetry and impedance spectroscopy.

Atenolol oxidation was performed on two decades of concentration (10^{-6} - 10^{-4}) with a detection limit of $3.9 \times 10^{-7} M$.

From the impedance spectroscopy measurements an equivalent electric circuit in good agreement with experimental data has been put up. It allows to determine the electrical parameters.

In Chapter 5 of this paper it is presented the study of carbamazepine oxidation using a gold electrode modified with graphene and gold nanoparticles, by linear voltammetry and impedance spectroscopy. An equivalent circuit, in good agreement with experimental data has been suggested, which allows to determine the electrical parameters.

Chapter 1. General behaviour of enzyme catalyzed reaction and their monitorization

1.1. Kinetics of enzyme catalyzed reactions

The enzymes are very efficient catalyst, and can act at extremely low concentration [1]. Here we present the most simple mechanism involving only one substrate. The kinetic measurements consist of measuring the rate of enzymatic reaction for various mixtures containing increased concentration of substrate and constant concentration of the enzyme.. This kind of measurements are used to show the dependence of the rate on substrate concentration and the aspect of curve is that in figure 1.1.1. In the range of large concentration of substrate a maximum limit (r_{\max}), is attained. Its values depends linearly on the concentration of enzyme $[E]_0$.

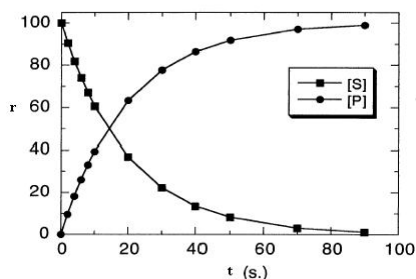


Figura 1.1.1. The plot of the initial reaction velocities as a function of substrate at constant enzyme concentration .

This behaviour has been described by Michaelis and Menten, by a simple mechanism [2] having an intermediate enzyme-substrate complex:



S and P stand for the substrate and the product respectively, ES symbolize the intermediate complex..The rate law has the following form:

$$r = [S] \frac{k_2 [E]_0}{[S] + \frac{k_{-1} + k_2}{k_1}} = \frac{r_{\max} [S]}{[S] + K_M} \quad (1.1.8)$$

It is in accordance with the experimentally diagrams presented in figure 1.1.1. The ratio comprising the three rate constants, two of first order, and one of second order, considering the formation of product in the within the initial part of the reaction $(k_{-1} + k_2)/k_1 = K_M$ is designed as Michaelis constant of the substrate. Although it is named as a constant K_M , it is not an thermodynamic equilibrium constant. It defines the steady-state of intermediate ES complex concentration. Several types of linear dependence lead to these parameters.

1.3. Inhibition of enzyme catalyzed reactions

Various substances present in the reaction mixture diminish or suppress the rate of enzymatic reactions and are named inhibitors. The effect of them on the reaction rate is characterized by several parameters as dissociation constants of enzymatic species, the inhibition fraction or ratio (relative potential of inhibition) and the inhibitor concentration that reduces the to one half of the uninhibited reaction.

The inhibitors are classified by Committee of International Union of Biochemistry (IUB), [15] in various types after their effects on the Michaelis parameters as: competitive, uncompetitive, noncompetitive and mixed. The difference between various types of inhibition are deduced by linear dependence described by Lineweaver and Burk.

The most general inhibition mechanism describes the interaction between substrate and enzyme, inhibitor and enzyme and the subsequent interaction EI-S and ES-I. It is shown in the figure 1.3.1, and comprise the symbols of the involved species as well as the constants

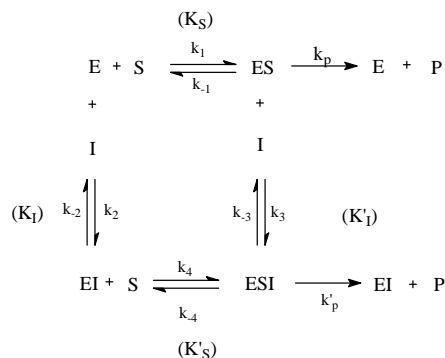


Figura. 1.3.1. The general inhibition mechanism

Chapter 2. The inhibitory effect of phenol on the peroxidase-catalyzed decomposition of hydrogen peroxide

The decomposition reaction of hydrogen peroxide catalyzed by peroxidase has been investigated amperometrically, in the presence of various concentrations of phenol and by using a Clark oxygen sensor. Comparative measurements were additionally performed by using an extract from horseradish peroxidase.

2.1. Peroxidase: general presentation

Peroxidase (EC 1.11.1.7) which belongs to the class of oxidoreductases, catalyzes the oxidation of phenol and its derivatives using either hydrogen peroxide or an organic peroxide as an oxidizing agent. [24].

The structure, kinetic mechanism and specificity of various plant peroxidases are well known, particularly those from *Armoracia* sp. (horseradish peroxidases) and *Arabidopsis thaliana*.

2.9. Principle of amperometric method

The measurements were undertaken with a Clark oxygen sensor, attached to a Multiline P4 multimeter with automatic data acquisition on a PC. All experiments were performed in a vessel provided with a water jacket. The temperature was maintained constant at 20 ± 0.1 °C, by means of a Falc 90 recirculatory water bath. The reaction mixtures were stirred with a magnetic stirrer, always with the same frequency.

The initial reaction rate, r_0 , was determined from the slope of the early part of O_2 evolution curve, after peroxidase addition. The well-known Michaelis-Menten equation describes the dependence of rate (r_0) on substrate concentration: This equation can be brought into the double-reciprocal form, also known as Lineweaver-Burk plots.

$$\frac{1}{r_0} = \frac{1}{r_{\max}} + \frac{K_M}{r_{\max}} \cdot \frac{1}{[S]} \quad (2.9.2)$$

The values obtained by us for Michaelis-Menten constant ($K_M = 4.25 \times 10^{-3}$ mol/L) and the maximum velocity ($r_{\max} = 2.88 \times 10^{-6}$ mol/Ls) are comparable to those mentioned in the literature.

When the concentration of H_2O_2 was varied at several fixed concentration of phenol, which has inhibitory effect, Lineweaver-Burk plots resulted in a family of straight lines (Fig.2.9.2).

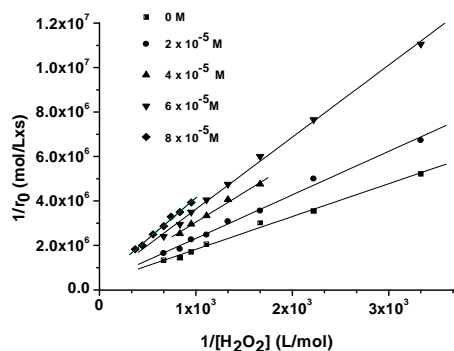


Figure 2.9.2. Lineweaver-Burk plots for H_2O_2 decomposition in the presence of various concentration of inhibitor

In table 2.9.2 are presented the values of kinetic parameters $r_{\max(I)}$ and $K_{M(I)}$ at different concentration of phenol, obtained from the linear regression. It is obvious from this table that the maximum velocity decreases with increasing phenol concentration, confirming the inhibitory effect of phenol

Table 2.9.2. Mean values of the maximum velocity $r_{max(I)}$ and Michaelis Menten constant in the presence of the inhibitor $K_{M(I)}$

| $10^5 \times [\text{phenol}]_0$ (mol/L) | slope | $10^6 \times r_{max(I)}$ (mol/Ls) | Intercept | $10^3 \times K_{M(I)}$ (mol/L) | R/n |
|--|-------|--------------------------------------|-----------|-----------------------------------|--------|
| 0.0 | 1476 | 2.88 | 346166 | 4.25 | 0.1424 |
| 2.0 | 1958 | 2.80 | 356482 | 5.48 | 0.1245 |
| 4.0 | 2671 | 2.65 | 376526 | 7.07 | 0.1991 |
| 6.0 | 3241 | 2.59 | 386030 | 8.39 | 0.1248 |
| 8.0 | 3724 | 2.39 | 417863 | 8.90 | 0.1424 |

The constant K_I of EI was obtained from the slope of $K_{M(I)}/r_{max(I)}$ versus [phenol] plot and a value of $(4.77 \pm 0.97) \times 10^{-5}$ mol/L was obtained. The constant K_I' of EIS was obtained from the intercept of $1/r_{max(I)}$ versus [phenol] plot and a value of $(3.35 \pm 0.97) \times 10^{-4}$ mol/L was obtained. (table 2.9.3).

The inhibition constants ratio K_I/K_I' is $\sim 10^{-1}$ meaning that the affinity of the enzyme for the inhibitor is higher than that of ES complex.

Dissociation constant values obtained by mathematical method, $K_I = (5.43 \pm 0.50) \times 10^{-5}$ mol/L and $K_I' = (5.54 \pm 0.97) \times 10^{-4}$ mol/L, are in good agreement with those obtained by graphical method.

Dissociation constant values: K_I and K_I' , show in table 2.9.3, was determined with equations (1.3.15) and (1.3.16.), with $\beta = 0$, and using apparent Michaelis Menten constants in the presence of the inhibitor.

Table 2.9.3. Dissociation constant values K_I , K_I'

| $[\text{phenol}]_0 \times 10^5$ (mol/L) | $K_I \times 10^5$ (mol/L) | $K_I' \times 10^4$ (mol/L) | $\overline{K_I} \times 10^5$ (mol/L) | $\overline{K_I'} \times 10^4$ (mol/L) |
|--|------------------------------|-------------------------------|---|--|
| 2.0 | 6.11 | 6.82 | 5.43 | 5.55 |
| 4.0 | 5.00 | 4.94 | | |
| 6.0 | 5.11 | 5.79 | | |
| 8.0 | 5.50 | 4.65 | | |

Table 2.9.3 shows an inconsistency of inhibition constants K_I și K_I' . This is due to the fact that β coefficient is not zero. Therefore the inhibition is not total. The average values resulted from the calculus are: $K_I = 5.4 \cdot 10^{-5}$ mol/L and $K_I' = 5.55 \cdot 10^{-4}$ mol/L.

The Lineweaver-Burk plots converge to a common intersection on the left side of the ordinate and above the abscissa ($x = -3528$ L/mol, $y = 777673$ Ls/mol) which correspond to the inhibition pattern of full or partial mixed inhibition.: [49]

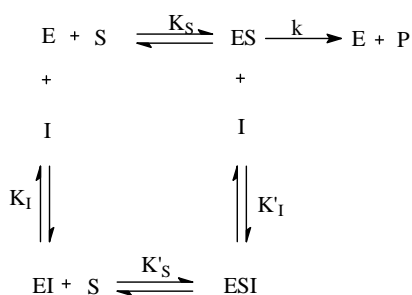


Figure. 2.9.4. Representation of fully mixed inhibition or noncompetitive inhibition.

Figure 2.9.9 show two typical kinetic curves, at the identical concentrations of H_2O_2 with peroxidase (blue), and horseradish peroxidase (pink).

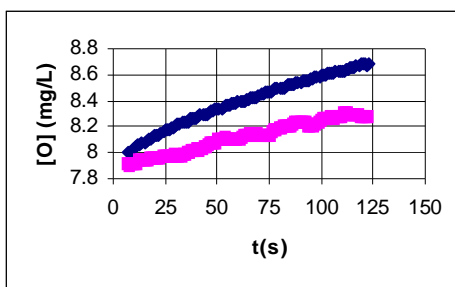


Figure 2.9.9 Two typical kinetic curves showing the O_2 evolution during the reaction (pH 7 and $20^{\circ}C$) with peroxidase (blue), and horseradish peroxidase (pink)

In the case of horseradish peroxidase, the determination of K_M and r_{max} parameters was difficult to achieve, due to the lack of reproducibility of the experimental measurements. The enzyme activity modifies within the measurement time, even if the extract was kept in the refrigerator. Different batches of extracts lead to different results because of different enzyme concentration

Chapter 3. Kinetic determination of drug concentration via enzyme-catalyzed decomposition of hydrogen peroxide

Catalase (oxidoreductase, EC 1.11.1.6.) is a very efficient catalyst for the decompositions of H_2O_2 , which also catalyzes the oxidation of primary alcohols, phenols, sodium nitrite, sodium azide and hydroxylamine by H_2O_2 (peroxidatic reaction). Is a tetrameric haemin-enzyme consisting of a 4 identical tetrahedrally arranged subunits of 60000 g/mol each.

Some aliphatic hydroperoxides can also support the peroxidatic reactions of catalase . This reaction is know under name catalitic activity [55].



3.3. Drug used as inhibitors of hydrogen peroxide decomposition reaction

One of the most charming areas of modern enzymology is the application of enzyme inhibitors as drugs in human and veterinary medicine. For example, aspirin, one of the most popular drug in the world, used as an antiinflammatory, acts like a prostaglandin synthetase enzyme inhibitor [59].

3.5. Atenolol, Metoprolol. General presentation

Atenolol is a cardioselective β -adrenoceptor blocking agent (β -blocker). *Atenolol* ($C_{14}H_{22}N_2O_3$) is conform with Pharmacopee Europeene (\pm)-2-[4-(2-hydroxi-3-izopropylaminopropoxil)]-phenyl]-acetamide.[110]

Metoprolol ($C_{34}H_{56}N_2O_{12}$) is a cardioselective β -adrenoceptor blocking agent (β -blocker). Its formula is (\pm)-1-isopropyl-amino-3-p-(2-methoxyethyl)- phenoxypropan-2-ol (2R,3R)-tartrate, having the number 56392-17-7, in accordance to British Pharmacopeia [110] *Atenolol* and *Metoprolol* are frequently prescribed blood pressure-control medications. Both drugs have an inhibitive effect on the catalytic decomposition of hydrogen peroxide with catalase.

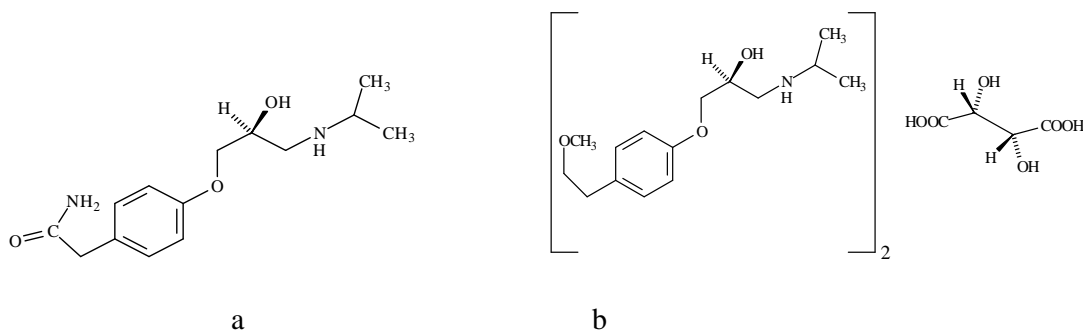


Figure 3.5.1. Chemical structure of: atenolol (a); metoprolol tartrate (b)

These drugs are used in clinical medicine for the treatments of various diseases including hypertension, pectoral angina, cardiac aritmia and especially ventricular tahicardic and hart attack.

3.9. Results and discussions

In the ultraviolet range, the decomposition of H_2O_2 by catalase can be directly followed by the decrease in the absorption peak at 240 nm. Metoprolol and atenolol have no interference effect, due to the fact that their absorption peaks appear at 273 respectively 270 nm (Fig.3.9.1).[127]

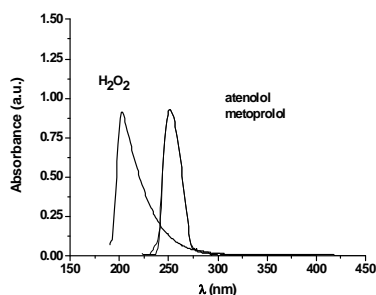


Figure 3.9.1. UV spectra of H_2O_2 , atenolol, and metoprolol

Figure 3.9.1. show UV spectra of H_2O_2 , atenolol and metoprolol.

The reaction of decomposition of H_2O_2 catalyzed by catalase takes place involving a simple first-order kinetic.

Measurements were performed in the presence of each drug (atenolol or metoprolol), for five initial concentration of H_2O_2 , at constant enzyme concentration of 1.8×10^{-10} mol/L in order to obtain the Michaelis-Menten kinetic parameters. The absorbance change for H_2O_2 disappearance obeys a first order dependence up to 600s of reaction time. Determination of kinetic parameters was done by processing the time curve versus absorbance using Table Curve program. Means values of initial velocities were calculated from 3 independent measurements under the same experimental conditions. The first-order rate constants were calculated from the fitted curves with the corresponding kinetic equation.

The value of the Michaelis-Menten constant ($K_M = 4.49 \times 10^{-2}$ mol/L) and the maximum rate ($r_{max} = 4.12 \times 10^{-3}$ mol/Ls) obtained by us for metoprolol are comparable to those mentioned in the literature [48]. For atenolol these values are smaller ($K_M = 2.89 \times 10^{-2}$ mol/L; $r_{max} = 9.7 \times 10^{-4}$ mol/Ls) but they also agree well with previous values reported before. When the concentration of H_2O_2 was varied at several fixed concentration of metoprolol ($0 - 6 \times 10^{-6}$ M) or atenolol ($0 - 8 \times 10^{-6}$ M) the Lineweaver–Burk plots resulted in a family of straight lines (Fig.3.9.2. respectively Fig.3.9.3).

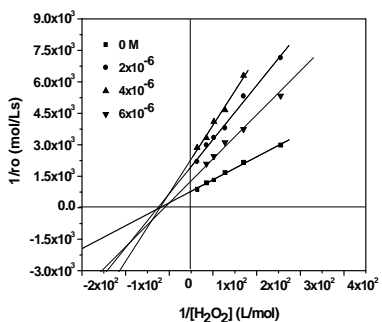


Figure.3.9.2. Lineweaver-Burk plots for H_2O_2 decomposition in the presence of various concentration of metoprolol

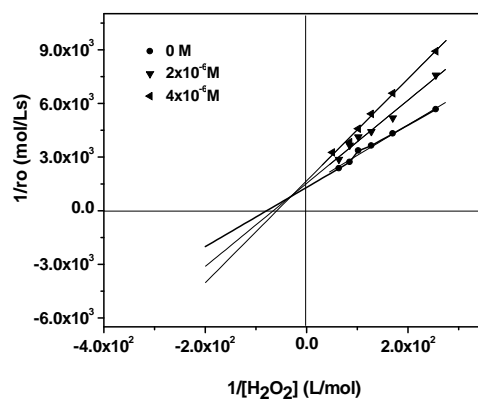


Figure.3.9.3. Lineweaver-Burk plots for H_2O_2 decomposition in the presence of various concentration of atenolol

According to Gelpi et al., 1993, the mathematical relationships for the Michaelis–Menten parameters in the presence of the inhibitors (I) are:

$$r_{\max(I)} = r_{\max} \frac{1 + \beta \frac{[I]}{K_I}}{1 + \frac{[I]}{K_I}} \quad \text{and} \quad K_{M(I)} = K_M \left(\frac{1 + \frac{[I]}{K_I}}{1 + \frac{[I]}{K_I'}} \right) \quad (3.2)$$

where K_I is the dissociation constants of the enzyme-inhibitor complex (EI) and K_I' stands for the dissociation constant of inhibitor, as a ligand from the enzyme–substrate–inhibitor complex (ESI) [15] A full inhibition mechanism appears when the ternary complex ESI does not yield any product that means the inhibitor completely blocks the enzyme activity. On the contrary, partial mixed inhibition leads to product formation through ESI, at a far reduced rate (characterized by $k_i = \beta k$, with $\beta < 1$) as compared to non-inhibited reaction..

In figures.3.9.2 and 3.9.3, the Lineweaver-Burk plots converge to a common intersection on the left side of the ordinate and above the abscissa, which according to Gelpi et al., 1993, corresponds to mixed inhibition. The values of kinetic parameters $r_{\max(I)}$ and $K_{M(I)}$ were determined from linear regression at different concentration of metoprolol or atenolol and are shown in Table 3.1. It is obvious from these tables that the maximum rate decreases with increasing inhibitor concentration, confirming its inhibition effect.

Table 3.1 Mean values of the maximum rate $r_{\max(I)}$, Michaelis Menten constant $K_{M(I)}$ and dissociation constant (K_I, K_I') for metoprolol and atenolol.

| $C \times 10^6$ (mol/L) | 0.0 | 2.0 | 4.0 | 6.0 | 8.0 |
|---------------------------------------|------|------|------|------|------|
| [metoprolol] | | | | | |
| $r_{\max(I)} \times 10^3$ (mol/Ls) | 4.12 | 1.76 | 1.48 | 1.45 | - |
| $K_{M(I)} \times 10^2$ (mol/L) | 4.49 | 3.30 | 3.38 | 4.71 | - |
| $K_I \times 10^5$ (mol/L) | 5.76 | | | | |
| $K_I' \times 10^4$ (mol/L) | 4.14 | | | | |
| [atenolol] | | | | | |
| $r_{\max(I)} \times 10^4$ (mol/Ls) | 9.70 | 9.48 | 7.14 | 6.82 | 6.53 |
| $K_{M(I)} \times 10^2$ (mol/L) | 2.89 | 2.34 | 1.21 | 2.02 | 1.51 |
| $K_I \times 10^5$ (mol/L) | 5.36 | | | | |
| $K_I' \times 10^4$ (mol/L) | 2.58 | | | | |

Our experimental results have shown that the values obtained from UV spectroscopy are two times larger than those obtained with Clark electrode, under the same experimental conditions. This is due to the fact that the hydrogen peroxide consumption is to times greater than the molecular oxygen release.

Consequently, we have determined the dissociation constant of enzyme-inhibitor complex (K_I) from the slope of $K_{M(I)}/r_{\max(I)}$ versus [inhibitor] plot (in this case metoprolol or atenolol, see Fig.3.9.4 a,b). The dissociation constant of enzyme-inhibitor-substrate complex (K_I') was obtained from the intercept of $1/r_{\max(I)}$ versus [inhibitor] plot (Fig.3.9.5 a,b).

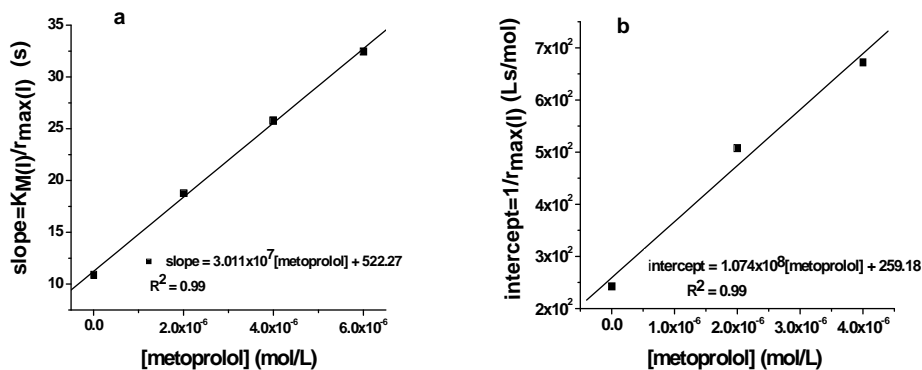


Figure 3.9.4 Linear dependence of the slope of Lineweaver-Burk plots on the metoprolol concentration, used for the determination of inhibitor constant, K_I (a); Secondary plot of the intercept of Lineweaver-Burk plots on the metoprolol concentration, used for the determination of inhibitor constant, K_I' (b).

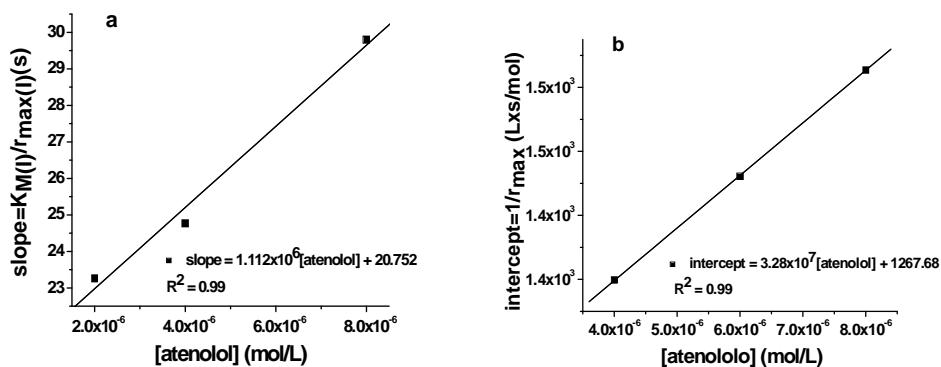


Figure 3.9.5 Linear dependence of the slope of Lineweaver-Burk plots versus atenolol concentration, used for the determination of inhibitor constant, K_I (a); Secondary plot of the intercept of Lineweaver-Burk plots versus atenolol concentration, used for the determination of inhibitor constant, K_I' (b).

These values are summarized in Table 3.1 and it can be seen that the inhibition constants have a ratio $K_I/K_I' \sim 10^{-1}$ which means that the affinity of the enzyme for the inhibitor is higher than the affinity of the enzyme for the substrate.

Based on these observations, the mechanism proposed for inhibition of catalase by metoprolol or atenolol, during decomposition of hydrogen peroxide, corresponds to one of mixed inhibition.

Chapter 4. Study of Atenolol oxidation by using a glasy carbon electrode, modifield with multicomponent nanostructural assembly of amino acids and gold nanoparticles

The employment of modifield electrodes exhibits various application in a wide variety of areas of analysis: medicine, pharmacy, environmental protection, food processing, military equipment.

Gold nanoparticles (AuNPs) have been intensively used for surface modification, due to their promising electrocatalytic and sensor applications [137-139].

Recently, many studies were focused on atenolol detection due to its therapeutic use in the treatment of angina pectoris, myocardial infarct as well as for hypertension or cardiac arrhythmia [145,147].

Original contributions

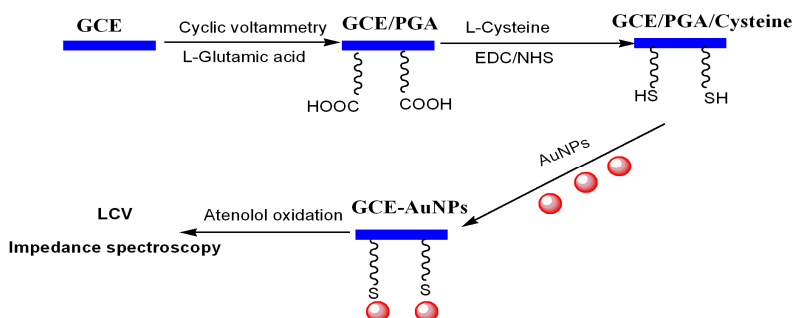
4.2. Preparation of citrate-capped gold nanoparticles (AuNPs)

Citrate-capped gold nanoparticles (AuNPs) were prepared as follows: 50 ml of HAuCl_4 (0.01 %) was brought to boil under constant stirring. Then, 1 ml of 1% trisodium citrate was

added and the mixture was boiled for about 15 minutes. Then, the solution was allowed to cool under vigorous stirring for about 45 minutes. TEM images revealed that the mean diameter of AuNPs was ≈ 40 nm.

4.3. Preparation of GCE modified with AuNPs (GCE-AuNPs)

The schematic representation of GCE modification is shown in schema. 4.4.



Scheme 4.4. Schematic representation of the attachment of gold nanoparticles to GCE.

Such structure is obtained GCE/PGA/cysteine/AuNPs, which will be symbolized GCE-AuNPs

4.4. Apparatus

Transmission Electron Microscopy images were collected on a field emission JEOL-JEM 1010 instrument (JEOL Inc.) equipped with a CCD camera.

Atomic Force Microscopy imaging was performed in the air in tapping modeTM using an Alpha 300A instrument (Witec) and silicon cantilever (43 Nm^{-1} spring constant; 317 kHz resonance frequency).

Cyclic Voltammetry, Linear Sweep Voltammetry and Electrochemical Impedance Spectroscopy measurements were performed by using a Versastat 3 Potentiostat (V3 Studio Software, Princeton Applied Research) connected with a three-electrode cell

4.5. Results and discussions

The modification of GCE with amine-containing compounds for sensor or electrocatalytic purposes has been intensively studied before [150-155].

Figure 4.5.3.shows a TEM image of gold nanoparticles on a copper grid. As we have expected from the pink color of the solution, they are well dispersed and have the diameter between 40 and 50 nm.

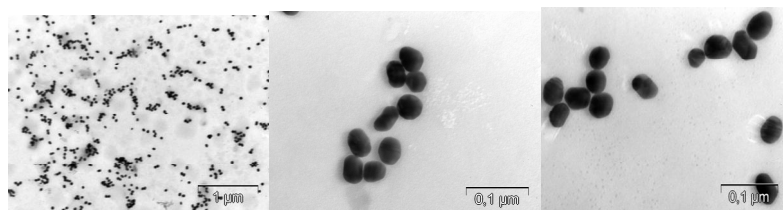


Figure 4.5.3 TEM image of citrate-capped gold nanoparticles on copper grid

After attachment to GCE surface (tapping modeTM AFM image, fig.4.5.5) they were forming larger agglomerates (size between 100 and 200 nm) which proved to have an excellent electrocatalytic activity for atenolol oxidation.

Figure 4.5.3 presents AFM images are obtained in "contact mode". It is noted that there is a high density of nanoparticles attached to surfaces

Figure 4.5.3 presents the images of the surface obtained by AFM contact mode . It can be noticed that there is a large density of gold nano-particle attached to on the surface of the electrode

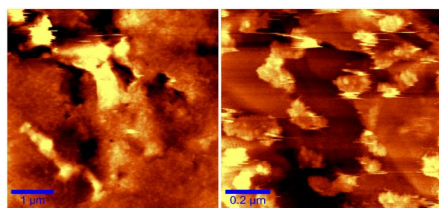


Figure.4.5.4. Contact^{CM} mode AFM image of GCE/AuNPs surface

Image much clearer were obtained when one used the tapping mode . As show in Figure 4.5.4, the electrode surface was covered with a monolayer of metal nanoparticles. Nanoparticles have generally kept the original size (that of colloidal solution) and only few cases have formed larger conglomerates (dimensions>100nm)

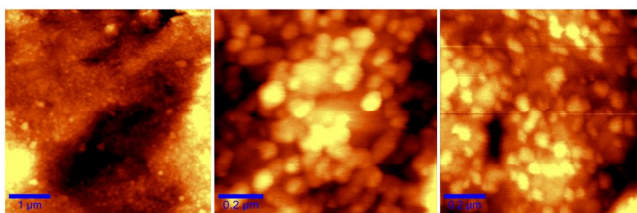


Figure 4.5.5. TappingTM mode AFM image of GCE/AuNPs surface.

4.6. Electrochemical characterization, GCE-AuNPs

After the modification of GCE with gold nanoparticles, the electrode was thoroughly rinsed with de-ionized water to remove loosely bound nanoparticles and then transfer to 0.04 M Britton-Robinson buffer solution, pH 9.5. Linear sweep voltammetry was recorded in the

potential range between 0.3V to 1 V/SCE at a scan rate of 50 mVs⁻¹ (Fig.3). As expected, no redox peak was evidenced in this buffer. Subsequently, the electrode was transferred to BR buffer solutions containing various concentration of atenolol (10⁻⁷-10⁻³ M). The electrocatalytic activity of the nanostructured assembly has allowed the detection of atenolol oxidation peak at around + 0.65 V/SCE (Fig.3). This potential is significantly lower than that obtained with a C₆₀-modified GCE (+1.04 V vs Ag/AgCl) or nanogold-modified carbon paste electrode (+ 0.85 V vs Ag/AgCl) [145, 147].

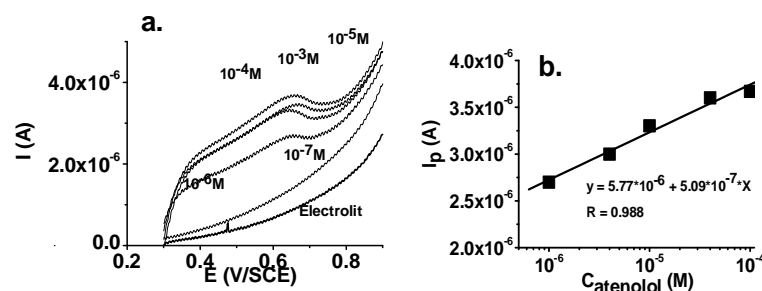


Figure 4.5.6. Linear sweep voltammetry recorded in BR buffer as well as in buffer containing various concentration of atenolol (10⁻⁷-10⁻³ M) (a); variation of I_p with atenolol concentration (b).

LCVs measurements show the enhancement of current peak with atenolol concentration. It is interesting to emphasize that at higher atenolol concentrations (10⁻³ or 10⁻² M) the peak intensity markedly decreased. This can be attributed to the adsorption of the oxidation product on the electrode surface, which diminishes the active surface area [157]. A calibration plot was obtained by representing the peak current intensity versus atenolol concentration (Fig. 4.5.6b). The linear detection range was between 10⁻⁶ and 10⁻⁴ M. No oxidation peak was detected at 10⁻⁷ M atenolol concentration

Figure 4.5.12 shows LCVs recorded in Britton-Robinson buffer of various pH, each containing 6 x 10⁻⁴ M atenolol (scan rate 100 mVs⁻¹). The recording obtained in basic solution (pH 10) exhibits a single peak (at + 0.65 V/SCE) which can be assigned to the oxidation of amino group. The lack of any peak in acidic or neutral media support the finding that protonated amino group cannot be electrochemically oxidized.

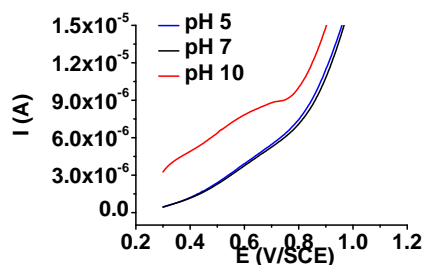


Figura 4.5.12 Linear sweep voltammetry recorded in Britton-Robinson buffer of various pH, each containing 6 x 10⁻⁴ M atenolol; scan rate 100 mVs⁻¹

In order to prove the electrocatalytic activity of electrode modified with gold nanoparticles, we have recorded LCVs using bare GCE (atenolol concentration from 10^{-7} to 10^{-3} M, see Figure 4.5.13).

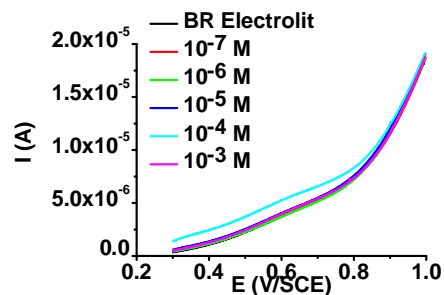
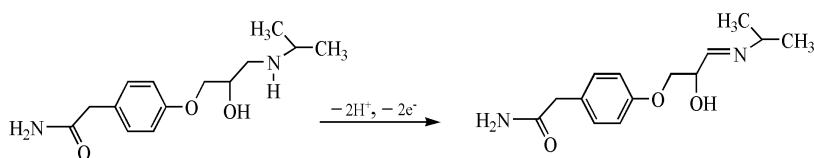


Figura 4.5.13 Linear sweep voltammetry recorded in BR buffer, as well as in buffer containing various concentrations of atenolol (10^{-7} - 10^{-3} M), using bare GCE; scan rate 50 mVs^{-1}

At low concentration (10^{-7} - 10^{-5} M) all LCVs have overlapped with the background recording, indicating a lack of sensitivity toward atenolol. At higher concentration (10^{-4} M) the current has increased and a very broad wave appeared around $+0.65 \text{ V/SCE}$, suggesting slow electron transfer kinetics. No peak was recorded at even higher concentration (10^{-3} M) and the current decreased, most probably due to the adsorption of the oxidation product on the electrode surface. Such findings clearly demonstrate the advantages of using gold nanoparticles attached to GCE surface.



Scheme 4.6 The proposed mechanism for electro-oxidation of atenolol on GCE-AuNPs electrode [147].

Oxidation occurs by transfer of 2 electron and 2 proton. The transfer of the two proton is from NH-group and not from the $-\text{OH}$ -group.[147].

Besides LSVs we have recorded EIS impedance spectra in BR buffer containing various concentrations of atenolol (from 10^{-6} to 10^{-3} M) at a potential of $+0.9 \text{ V/SCE}$ (see the electrical equivalent circuit and Nyquist diagram represented in Fig.4 5.14a,b). The EIS spectra recorded at higher atenolol concentration (10^{-3} - 10^{-2} M) have overlapped with that registered at 10^{-4} M and for clarity reason it was not shown in fig. 4b.

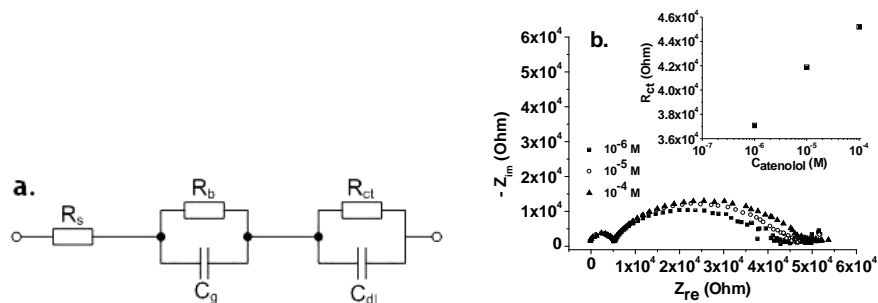


Figure 4.5.14. Equivalent electrical circuit employed to fit the experimental EIS spectra (a); Nyquist diagrams obtained at various concentrations of atenolol (10^{-6} ... 10^{-4} M) in BR buffer; inset: variation of R_{ct} with atenolol concentration (b).

All the spectra are characterized by two semicircles, a small one which appears at very high frequencies and a large one which appears at medium-low frequencies. The Warburg diffusion region (straight line, at an angle of 45°) is not well defined in the impedance spectra and therefore it was not taken into consideration in our model. The equivalent electrical circuit (Fig. 4.5.14a) employed to fit the EIS experimental data contains the solution resistance (R_s) and two parallel RC pairs: R_b , C_g respectively R_{ct} , C_{dl} .

Chapter 5. Novel Graphene-Gold Nanoparticle Modified Electrodes for the High Sensitivity Electrochemical Spectroscopy Detection and Analysis of Carbamazepine

A novel graphene-gold nanoparticle composite deposited on gold electrode (Au-Gr-AuNPs) was employed to detect carbamazepine (CBZ), an antiepileptic drug. The presence of gold nanoparticles encased in graphene sheets was evidenced by TEM and HRTEM. AFM analysis was used to study the morphology of the graphene-gold nanoparticles films used for the electrochemical studies. Various electrochemical methods were employed to study CBZ oxidation, such as Cyclic Voltammetry, Linear Sweep Voltammetry, and Electrochemical Impedance Spectroscopy.

Carbamazepine (Figure 5.1.1.) is a tricyclic compound used as an anticonvulsant drug for the treatment of epilepsy and bipolar disorder, as well as trigeminal neuralgia.

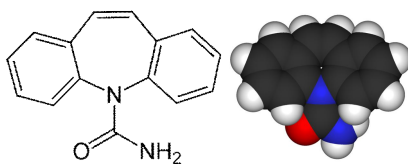
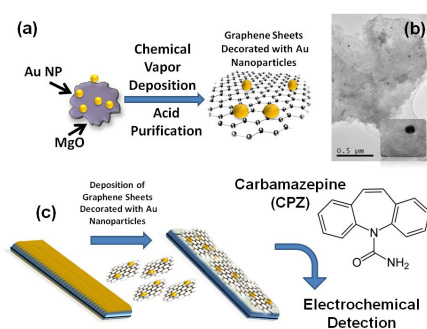


Figure 5.1.1. Carbamazepine chemical structure

Carbamazepine is currently considered one of the emerging pollutants in ground and surface water; therefore, its accurate determination by fast and reliable methods is highly desirable.

5.3. Preparation of gold electrode modified with graphene-AuNPs (Au-GR-AuNPs)

The schematic of the process presented by this paper is shown in scheme 5.1.a. The Au/MgO catalyst was found to synthesize graphene-AuNPs structures composed of 2-6 sheets and diameters of $600 \text{ nm} \pm 100 \text{ nm}$. An interesting observation was the fact that, during the growth process, the Au nanoparticles initially supported on the MgO were lifted off by the graphene sheets during the growth process and became encased in their crystalline structure (scheme. 5.1.b). The size of these Au nanoparticles was found to be relatively uniform with diameters between 10 and 20 nm. The inset of scheme 5.1.b shows the higher magnification of such a nanoparticle encased in the graphitic structure of the graphene sheets. The graphene-AuNPs composite were further solubilized and deposited onto the top surface of a gold electrode used for electrochemical studies (scheme.5.1.c).



Scheme 5.1 Schematic representation of the synthesis of graphene decorated with Au nanoparticles by RF-CCVD over an Au/MgO catalyst (a); transmission electron analysis (TEM) (80 kV) of the resulting structures (b); schematic of the process used to deposit graphene-AuNPs composite over the top surface of a gold electrode to be further used in an electrochemical setup for the detection of carbamazepine (c)

5.5. Results and discussions

Figure 5.5.1b,c,d provides a representative AFM image (TappingTM mode) which reveals graphene-AuNPs with various shapes and sizes.

Further analysis of graphene-AuNPs composite deposited onto gold surface reveals a clear tendency of these nanostructures to form large agglomerates. Previous studies have confirmed that water molecules intercalated between the platelets are forming hydrogen bonding to the epoxy or hydroxyl functionalities, being a key factor in maintaining the stacked structure of the graphene-like structures [180]. After their deposition on the gold electrode, the clusters of graphene-AuNPs composite suffer agglomeration with an average height of up to 1 micron without the single-sheet morphology, however.

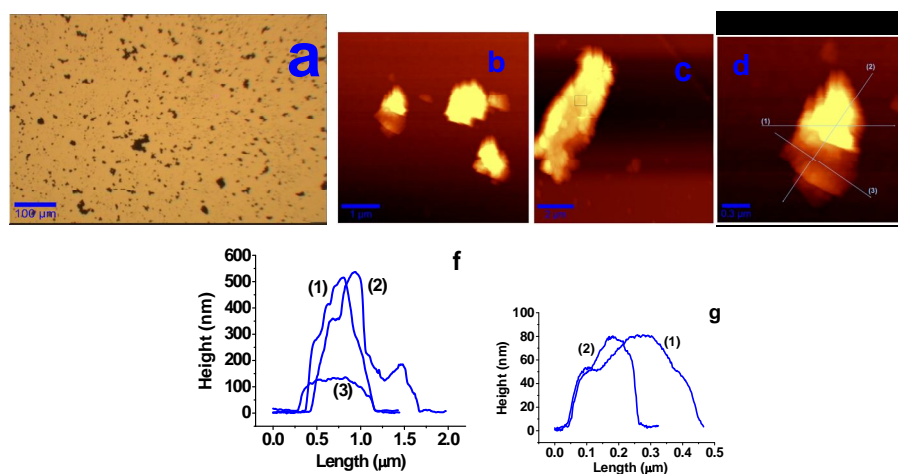


Figure 5.5.1. Optical image of modified surface gold electrode with graphene, Au-GR (a); representative image (TappingTM mode) which reveals graphene-AuNPs, with various shapes and sizes (b-d); transversal section, of graphene-AuNPs (f,g).

5.6. Electrochemical characterization

Since carbamazepine has a very low solubility in water (17.7 mg/L^{-1} at 25°C), in our studies we have chosen acetonitrile as solvent. Figure 5.6.1. shows successive cyclic voltammograms (3 cycles) recorded in the supporting electrolyte (acetonitrile + 0.05 M TBAP), as well as in electrolyte containing 10^{-2} M carbamazepine (scan rate $\nu = 25 \text{ mVs}^{-1}$). A two-wave oxidation peak can be seen at around $+1.49 \text{ V/Ag(AgCl)}$ accompanied by a small reduction peak at $+1.16 \text{ V/Ag(AgCl)}$. The large separation between the oxidation and reduction peaks ($\approx 330 \text{ mV}$) suggests that carbamazepine molecules undergo a quasireversible redox process. At a slow scan rate (between 5 and 50 mVs^{-1}), the redox process is diffusion-controlled as shown by I_{peak} versus $\nu^{1/2}$ plot. (See inset of Fig. 5.6.1.) This was further confirmed by the plot of $\log I_{\text{peak}}$

peak *versus* $\log v$, which was linear within the same scan rate range and gave a slope of 0.6 (data not shown).

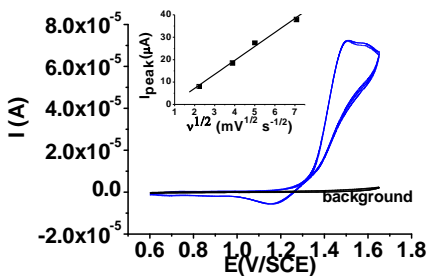


Figure 5.6.1. Successive cyclic voltammograms recorded with Au-GR-AuNPs electrode in supporting electrolyte (acetonitrile + 0.05 M TBAP- black line), as well as in electrolyte solution containing 10^{-2} M carbamazepine (three cycles, scan rate 25 mVs^{-1} - blue line); inset: variation of peak current intensity versus $v^{1/2}$ (diffusion-controlled process).

The successive cyclic voltammograms show that the electrochemical signal of carbamazepine is almost unmodified, suggesting that the electrode surface is not blocked by the adsorption of the oxidation products. However, in order to have reproducible results in our analytical determinations, the data obtained from the first scan (either CV or LCV) were always used.

The two-wave shape of the oxidation peak supports the electrochemical-chemical mechanism that carbamazepine molecules undergo during oxidation. This was observed by CV and LCV only at high concentrations (10^{-2} M); at lower concentrations, the two peaks overlap, generating a broad oxidation wave (see Fig. 5.6.1 and 5.6.2a). LCV measurements show the increase of the peak current with carbamazepine concentration (Fig. 5.6.2a). At low concentrations (10^{-6} M), the recording overlapped with the background. A clear increase in the peak current was obtained at higher concentrations, which allowed the plotting of a calibration curve between $5 \times 10^{-6} - 10^{-2}$ M range. (See Fig. 5.6.2.b.) A detection limit (DL) of 3.03×10^{-6} M was obtained in this case ($S/N = 3$).

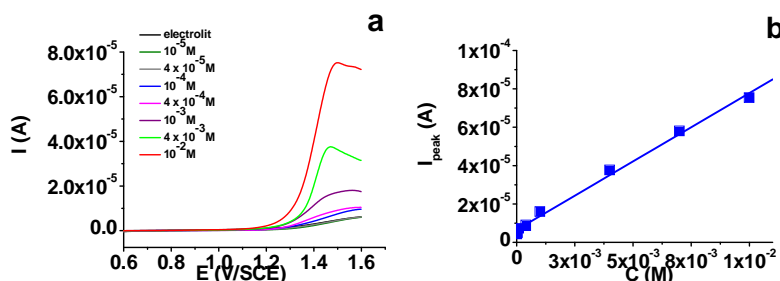


Figure 5.6.2 LCVs recorded with Au-GR-AuNPs electrode in electrolyte containing various concentrations of carbamazepine ($10^{-5} - 10^{-2}$ M); scan rate 25 mVs^{-1} (a); variation of peak current intensity (I_{peak}) with carbamazepine concentrations within $10^{-5} - 10^{-2}$ M range (b).

In order to prove the electrocatalytic activity of the modified gold electrode, we also recorded LCVs using a bare gold surface (Fig.5.6.3, scan rate = 25 mVs⁻¹). A significant decrease in current (up to 2 times) was obtained with the bare electrode for all concentrations, along with a shift in the peak potential (≈ 100 mV to higher anodic potentials). For the sake of clarity, only two concentrations are shown here. Such findings reflect the enhancement of the electron transfer between carbamazepine molecules and the nanostructured surface and clearly demonstrate the advantages of using a graphene-AuNPs layer attached to gold substrate.

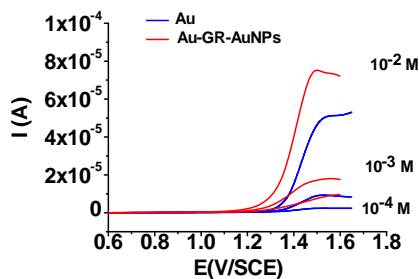


Figure 5.6.3. LCVs recorded with Au (blue line) and Au-GR-AuNPs electrode (red line), respectively, in electrolyte containing various concentrations of carbamazepine (10^{-2} and 10^{-3} M); scan rate 25 mVs^{-1}

A further characterization of the nanostructured electrode was performed by measuring the electrochemical impedance spectra at a potential of + 1.49 V/Ag(AgCl).

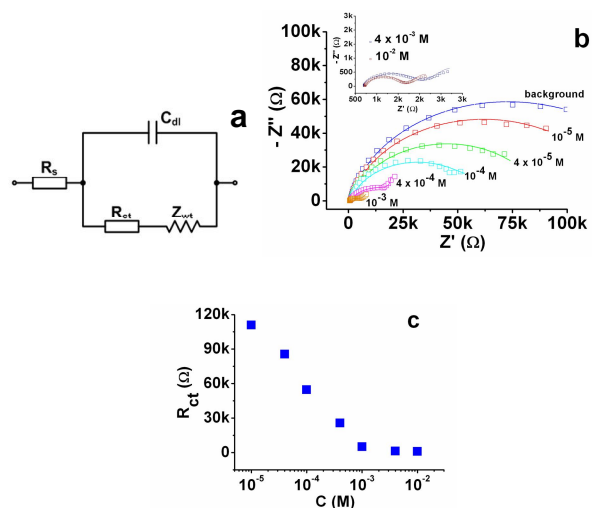


Figure 5.6.4. Equivalent electrical circuit employed to fit the experimental EIS spectra (a); Nyquist diagrams obtained with Au-GR-AuNPs electrode in electrolyte containing various concentrations of carbamazepine (10^{-5} – 10^{-2} M) at an applied potential +1.49 V/Ag/AgCl; the continue lines represent the fit based on the equivalent circuit (b); variation of R_{ct} with carbamazepine concentration (c).

The equivalent circuit and Nyquist plots is represented in Fig. 5.6.4 a,b). At the lowest

concentration (10^{-6} M), the spectrum overlapped with that obtained for the supporting electrolyte (background); therefore, only one curve was represented in this plot. The spectra are characterized by a single semicircle (high-medium frequency range) followed by a straight line at an angle of 45° , in the low frequencies range. Such a line corresponds to the Warburg diffusion region and, in our case, appears only for concentrations higher than 10^{-4} M. The equivalent electrical circuit (Fig. 5.6.4a) employed to fit the EIS experimental data contains the solution resistance (R_s), the charge-transfer resistance (R_{ct}), the Warburg impedance (Z_{Wt} - transmissive boundary), and the double-layer capacitance (C_{dl}).

The Nyquist plot (Fig. 5.6.4b) shows that, with increasing carbamazepine concentrations, the large semicircle due to the coupling between R_{ct} and C_{dl} gradually decreases. This can be attributed to a higher number of carbamazepine molecules that are oxidized at the electrode surface; consequently, the double-layer capacitance increases, and the imaginary part of the impedance (Z'') decreases. R_{ct} relates to surface modifications that hinder the transfer of electrons at the electrode/solution interface. In our case, one can see that R_{ct} has a linear variation with carbamazepine within the range of 10^{-5} – 10^{-3} M concentration (decreases from 110 to 5 k Ω); above 10^{-3} M, it exhibits a saturation tendency ($\sim 890 \ \Omega$, Fig. 5.6.4c). This saturation may be due to the accumulation of carbamazepine molecules within the graphene platelets, which in time leads to a poor electrical transfer between the graphene-AuNPs layer and gold substrate.

General conclusions

Enzymes are extremely efficient catalyst at very low concentrations. Just as classic catalysts, enzymes provide a way to react to us, with a much lower activation energy, but without changing the balance of reversible reactions.

Based on enzyme kinetic mechanism, interaction between enzyme and substrate can be established.

The catalytic decomposition of hydrogen peroxide was studied in the presence of different phenol concentration. Comparative measurements were performed, using both pure and extracted peroxidase from horseradish. A fully mixed inhibition mechanism (noncompetitive inhibition) was proposed to describe the decomposition of hydrogen peroxide. A kinetic method for the determination of phenol concentration on the basis of its inhibitory effect has been suggested.

The catalyzed decomposition of hydrogen peroxide by catalase was studied in phosphate buffer in the presence of cardioselective β -adrenoceptor blocking agent, metoprolol and atenolol.

Michaelis-Menten kinetic parameters (K_M and r_{max}) which are characteristic for the catalyzed reaction were determined using Lineweaver-Burk plot. The results obtained from spectrophotometric measurements were compared with those previously obtained from amperometric experiments and both of them agree well with the reaction stoichiometry. The inhibition mechanism proposed for the catalase-catalyzed decomposition of hydrogen peroxide corresponds to a mixed inhibition

Atenolol oxidation study was performed using a glassy carbon electrode, GCE whose surface was modified with amino acids and assembly of gold nanoparticles (AuNPs), by linear voltammetry and impedance spectroscopy. The design chosen by us allows the detection of atenolol oxidation peak at a considerably lower potential (+0.65 V/SCE) compared with previous reports. The linear detection range for atenolol was between 10^{-6} - 10^{-4} M with a detection limit of 3.9×10^{-7} M. In addition we have developed an equivalent electrical circuit to model the EIS data and to determine important parameters like bulk resistance (R_b) of PGA/cysteine/AuNPs assembly and charge-transfer resistance (R_{ct}). As expected, R_b has a constant value (5 k Ω) regardless of atenolol concentration while R_{ct} linearly increases with atenolol from 37 to 45 k Ω , within 10^{-6} - 10^{-4} M concentration range.

A novel graphene-gold nanoparticle composite deposited on gold electrode (Au-Gr AuNPs) was employed to detect carbamazepine (CBZ), an antiepileptic drug.

The modified electrode exhibited excellent electrocatalytic effect for oxidation of CBZ, reflected by a significant increase of the peak current (up to 2 times) and a shifting of the peak potential towards lower oxidation potential (~ 100 mV), compared with the unmodified electrode. The detection limit for carbamazepine was found to be 3.03×10^{-6} M (S/N = 3).

Additionally, an equivalent electrical circuit was developed to interpret and fit the experimental EIS data based on the solution resistance (R_s), the charge-transfer resistance (R_{ct}), the Warburg impedance (Z_{Wt} - transmissive boundary), and the double-layer capacitance (C_{dl}).

The result of personal research contributes to enriching the knowledge that refers to kinetic and electrochemical method of analysis of some drug based on catalyzed and enzyme reactions.

Selected references

1. I. Bâldea, Some Advanced Topics in Chemical Kinetics, **2000**, Cluj-Napoca University Press
2. L. Michaelis, M. L. Menten, "Die Kinetik der Invertinwirkung", *Biochem. Z.*, **1913**, 49, 333-369

14. Symbolism and Terminology in Enzyme Kinetic Recommendation (1981) of the Nomenclature Committee of the International Union of Biochemistry Reprinted in Eur. J. Biochem., **1982**, 128, 281-291
15. J. Lluis Gelpi, J. David, Halsall, A theoretical approach to the discrimination and characterization of the different classes of reversible inhibitors *Concept in Biochemistry*, **1993**, 70, 10, 805
24. K.R. Barber, M.J. Rodrigues-Maron, G.S. Shaw, *Journal Biochemical*, **1991**, 232,
48. P. George, The reactions of catalase in the presence of the notatin system, *Biochem. J.*, **1949**, 44(2) 197-205
49. R.J. Leatherbarrow, Use of nonlinear regression to analyze enzyme kinetic data: Application to situations of substrate contamination and background subtraction, *Anal. Biochem.*, **1990**, 184(2), 274-278.
55. B. Chance, An Intermediate Compound in the Catalase-hydrogen peroxide Reaction, *Acta Chem. Scand*, **1947**, 1, 236-267
59. I. Claiken, S. Rose, R. Karlsson, *Anal Biochem.*, **1991**, 201, 197
110. ****Pharmacopee Europeene*, 3^e edition, **1997**
127. **F. Pogacean**, I. Baldea, L. Olenic, S. Pruneanu, Kinetic determination of drug concentration via enzyme-catalyzed decomposition of hydrogen peroxide, *Particles science and technology*, **2011**, in press, **Doi 10.1080/02726351.2010.521234**
132. **F. Pogacean**, I. Baldea, F. Turbat, The inhibitory effect of the atenolol upon the enzyme catalyzed hydrogen peroxide decomposition, **2006**, *Studia Universitatis Babeş-Bolyai Chimia LI*, 1
137. M.C. Daniel, D. Astruc, Gold nanoparticles: assembly, supramolecular chemistry, quantum-size-related properties, and applications toward biology, catalysis, and nanotechnology, *Chem. Rev.*, **2004**, 104, 293
138. S. El-Deab, T. Ohsaka, An Extraordinary Electrocatalytic Reduction of Oxygen on Gold Nanoparticles-electrodeposited Gold Electrodes, *Electrochem. Commun.*, **2002**, 4, 288-292
139. R. Willner, Baron, B. Willner, Growing metal nanoparticles by enzymes, *Adv. Mater.*, **2006**, 18, 1109-1120
145. R.N. Goyal, V.K. Gupta, M. Oyama, N. Bachheti, Differential pulse voltammetric determination of atenolol in pharmaceutical formulations and urine using nanogold-modified indium tin oxide electrode, *Electrochem. Commun.*, **2006**, 8, 65-70
146. N. Goyal, S.P. Singh, Voltammetric determination of atenolol at C60-modified glassy carbon electrodes, *Talanta*, **2006**, 69, 932-937.

147. M. Behpour, E. Honarmand, S.M. Ghoreishi, Nanogold-modified Carbon Paste Electrode for the Determination of Atenolol in Pharmaceutical Formulations and Urine by Voltammetric Methods, *Bull.KoreanChem.Soc.* **2010**, 31, 4, 845-849
150. A.M.Yu, H.Y.Chen, Electrocatalytic oxidation of hydrazine at the poly(glutamic acid) chemically modified electrode and its amperometric determination, *Anal.Lett.*, **1997**, 30, 599-607
151. L.Zhang, Y.Sun, X.Lin, Separation of anodic peaks of ascorbic acid and dopamine at an α -alanine covalently modified glassy carbon electrode, *Analyst*, **2001**, 126, 1760-1763
152. D.P.Santos, M.F.Bergamini, A.G.Fogg, M.V.B.Zanoni, Application of a glassy carbon electrode modified with poly(glutamic acid) in caffeic acid determination, *Microchim.Acta*, **2005**, 151, 1-2, 127-134
153. G.Hu, Y.Liu, J.Zhao, S.Cui, Z.Yang, Y. Zhang, Selective response of dopamine in the presence of ascorbic acid on L-cysteine self-assembled gold electrode, *Bioelectrochemistry*, **2006**, 69, 254-257
154. D.P.Santos, M.V.B.Zanoni, M.F.Bergamini, A-M. Chiorcea-Paquim, V.C. Diculescu, A-M. Oliveira Brett, Poly(glutamic acid) nanofibre modified glassy carbon electrode: Characterization by atomic force microscopy, voltammetry and electrochemical impedance, *Electrochim. Acta*, **2008**, 53, 3991-4000
155. R.S. Deinhammer, M.Ho, J.W. Andereg, M.D.Porter, Electrochemical oxidation of amine-containing compounds: a route to the surface modification of glassy carbon electrodes, *Langmuir*, **1994**, 10, 1306-1313
157. R.N. Hegde, B.E. Kumara Swamy, B.S. Sherigara, S.T. Nandibewoor, Electro-oxidation of Atenolol at a Glassy Carbon Electrode, *Int. J. Electrochem. Sci.*, **2008**, 3, 302-314
180. Du Meng, Tao Yang, Kui Jiao, *J. Mater. Chem.*, Immobilization-free direct electrochemical detection for DNA specific sequences based on electrochemically converted gold nanoparticles/graphene composite film, **2010**, 20, 9253-9260

Published papers-on the matter

1. C. Muresanu, L.Copolovici, **F. Pogacean**, A kinetic method for para-nitrophenol determination based on its inhibitory effect on the catalatic reaction of catalase, *Central European Journal of Chemistry*, **2005**, 3(4), 592-604.
2. A. Orza, L. Olenic, S. Pruneanu, **F. Pogacean**, A.S. Biris, Morphological and electrical characteristics of amino acid-AuNP nanostructured two-dimensional ensembles, *Chem. Phys.*, **2010**, 373, 295
3. D. Vlascici, S.Pruneanu, L. Olenic, . **Pogacean** et all, Manganese(III) Porphyrin-based Potentiometric Sensors for Diclofenac Assay in Pharmaceutical Preparation, **2010**, *Sensors*, 10(10), 8850-8864
4. S. Pruneanu, **F. Pogacean**, C. Grosan, E.M.Pica, L.V. Bolundut, A.S. Biris, Electrochemical investigation of atenolol oxidation and detection by using a multicomponent nanostructures assembly of amino acids and gold nanoparticles, *Chem. Phys. Lett.*, **2011**, 504, 1-3, 56-61
5. **F. Pogacean**, I.Baldea, L.Olenic, S. Pruneanu, Kinetic determination of drug concentration via enzyme-catalyzed decomposition of hydrogen peroxide, *Particulates science and technology*, **2011**, in press, **Doi 10.1080/02726351.2010.521234**.
6. **F. Pogacean**, I Baldea, F. Turbat, The inhibitory effect of the atenolol upon the enzyme catalyzed hydrogen peroxide decomposition, **2006**, *Studia Universitatis Babes-Bolyai Chemia LI*, 1
7. **F. Pogacean**, I. Baldea, F. Turbat, Inhibitory effect of metoprolol upon catalase-H₂O₂ decomposition , used as potential kinetic method to determine the drug concentration, **2007**, *Studia Universitatis Babes-Bolyai*, LI, 2, 125-134

Patents

1. S. Pruneanu, **F Pogacean**, L. Olenic, Valer Almasan, **Method of making a glassy carbon electrode modified with a set-based nanostructured gold nanoparticles and L-cysteine** (patents-Nr. OSIM A/00635 / 04.07.2011

